Journal of Alloys and Compounds 502 (2010) 434–438

Contents lists available at ScienceDirect

Journal of Alloys and Compounds

journal homepage: www.elsevier.com/locate/jallcom

Effect of thickness on the microstructural, optoelectronic and morphological properties of electron beam evaporated ZnTe films

A.R. Balu [a,c], V.S. Nagarethinam [a,c], A. Thayumanavan [a,c], K.R. Murali [b,c], C. Sanjeeviraja [b,c], M. Jayachandran [b,c,*]

[a] Department of Physics, A.V.V.M Sri Pushpam College, Poondi, Thanjavur, India
[b] Electrochemical Materials Science Division[1], Central Electrochemical Research Institute, Karaikudi 630006, India
[c] Department of Physics, Alagappa University, Karaikudi 630003, India

ARTICLE INFO

Article history:
Received 18 February 2010
Accepted 26 April 2010
Available online 5 May 2010

Keywords:
II–VI
Semiconductor
Thin films
ZnTe

ABSTRACT

ZnTe films of different thicknesses were deposited on glass substrates at a substrate temperature of 300 °C. The thickness of the films varied in the range of 110–320 nm. The films exhibited cubic structure with preferential orientation in the (1 1 1) direction. A very high value of absorption co-efficient (10^4 cm^{-1}) is observed. Band gap values in the range between 2.23 and 2.38 eV are observed when the film thickness was varied between 320 and 110 nm, respectively. The refractive index values are found to vary between 2.68 and 2.90 for the films of different thicknesses. It has been observed that the conductivity increases continuously with temperature as well as with thickness. Laser Raman spectra showed the presence of peaks at 206.8 and 411.2 cm^{-1} corresponding to the first order and second order LO phonon of monophase ZnTe films. PL analysis confirmed the formation of monophase ZnTe films with nano grains.
© 2010 Elsevier B.V. All rights reserved.

1. Introduction

ZnTe is a promising material for pure-green light emitting diode, windows layer in tandom solar cells, and transparent conductive thin films [1]. ZnTe can be used for back contact layer (BCL) on p-CdTe absorber layer in CdTe based solar cells before its metallization because the valence-band offset between p-ZnTe and p-CdTe is less than 0.05 eV [2].

This direct bandgap nature of ZnTe with a value of 2.26 eV makes it a potential candidate for the fabrication of pure-green LED devices [3–6]. Because of its high electro-optic coefficient, ZnTe also promises to be useful in the production and detection of terahertz (THz) radiation [3,7]. Since there is only a small valence-band offset of 0.05 eV between ZnTe and CdTe, ZnTe can be used as a back contact material to obtain higher solar energy conversion efficiency in CdTe based solar cells [8]. Though some research groups have reported the fabrication of ZnTe based devices like LEDs and terahertz detectors, most of them have preferred highly sophisticated techniques like molecular beam epitaxy (MBE), metal organic chemical vapor deposition (MOCVD), etc. to obtain ZnTe films [3–8], electrodeposition from aqueous solutions [9,10]. ZnTe is a very attractive host for optoelectronic device realizations because of its sensitivity in the green spectral region (2.26 eV). Specifically, for bright light emitting diodes (LEDs), ZnTe is a technologically important material since the emission wavelength matches well with the maximum sensitivity of the human eye. Utilization of ZnTe thin films in device development were reported by the realization of LED prototypes [11,12], high-efficiency multi-junction solar cells [13], and terahertz (THz) devices [14]. In some reports the concept of laser crossing and all-optical laser transmission digitizing with GaAs [15,16], CdS [17] and InP has been successfully demonstrated [18]. In an earlier report on electron beam evaporated ZnTe films, the optical and dielectric properties were discussed [19]. The exploration of novel thin film materials and simple technique based technologies for future light-based communication systems, such as all-optical switches and hybrid device structures [20], have been the driving motivation for the present work. In this study, structural, optical, morphological and electrical properties of ZnTe films deposited by the electron beam (EB) evaporation technique are presented in detail.

2. Experimental

ZnTe films of varying thickness were deposited on glass substrates by keeping the substrate temperature constant at 300 °C. Commercial ZnTe powder (99.99% purity) was used as the source. The substrate temperature was fixed well below the decomposition temperature observed from the DTA results which indicated an exothermic peak at 437 °C due to the partial decomposition of ZnTe. The films were characterized by X-ray diffraction (XRD) studies using CuKα radiation form an Xpert

* Corresponding author at: Electrochemical Materials Science Division, Central Electrochemical Research, Institute, Karaikudi 630006, India. Tel.: +91 4565 227550.
E-mail address: mjayam54@yahoo.com (M. Jayachandran).
[1] (Council of Scientific and Industrial Research, New Delhi).

0925-8388/$ – see front matter © 2010 Elsevier B.V. All rights reserved.
doi:10.1016/j.jallcom.2010.04.191

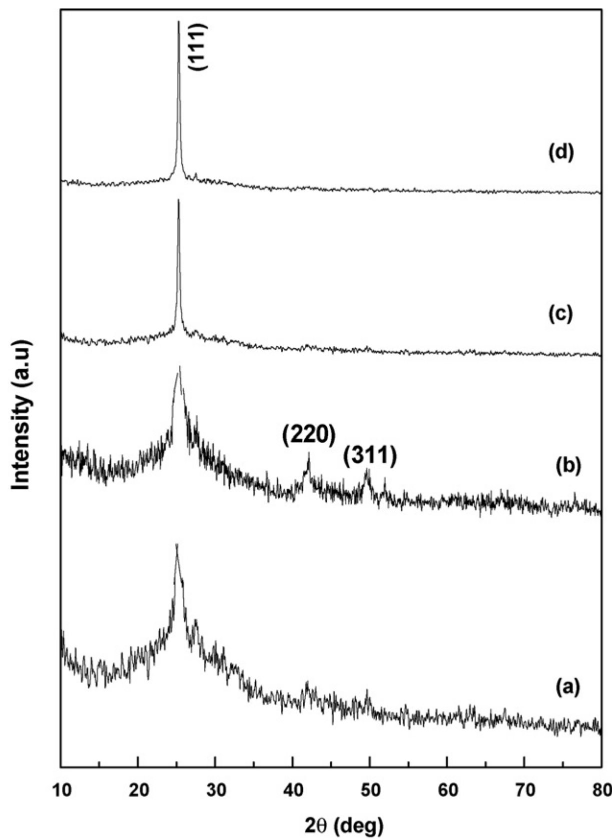

Fig. 1. X-ray diffraction patterns of ZnTe films of different thickness (a) 110 nm (b) 180 nm (c) 230 nm (d) 320 nm.

PANanalytical XRD unit. Optical studies were made at room temperature using a UV-Vis-NIR spectrophotometer.

Surface morphology of the films was studied by molecular imaging system atomic force microscope (AFM). Raman studies were made using Renishaw Invia Laser Raman microscope using a 18 mW 633 nm He–Ne laser. PL studies were made using Varian Cary Eclipse Fluorescence Spectrophotometer. Electrical resistvity was evaluated by providing Al contacts.

3. Results and discussion

The X-ray diffraction pattern (Fig. 1) shows that the ZnTe films of different thicknesses deposited at 300 °C substrate temperature possess cubic structure with an average lattice constant 'a' = 6.093 Å. The different peaks were indexed and the corresponding interplanar spacing 'd' were calculated and compared with the standard ASTM values. Preferential orientation in the (1 1 1) direction is also observed. The films deposited at room temperature indicate amorphous structure. As the deposition temperature increased, the peaks became sharper suggesting improved crystallinity. The thickness of the films estimated from Mitrutoyo surface profilometer was in the range of 110–320 nm. The microstructural parameters like grain size, strain and dislocation density have been calculated and are indicated in Table 1. The grain size was calculated using Scherrer's equation:

$$D = \frac{0.9\lambda}{\beta \cos\theta}$$

where D is the grain size, λ is the wavelength of CuKα radiation, θ is the diffraction angle and β is the full width at half maximum. The lattice strain (ε) is calculated using the relation,

$$\varepsilon = \frac{\beta \cos\theta}{4}$$

The value of dislocation density (δ) was calculated using the relation

$$\delta = \frac{15a}{\varepsilon D}$$

From the table, it is observed that grain size increases with thickness. Due to the increase in grain size with thickness, the defects in the lattice is decreased, which in turn reduces the stress, internal microstrain and dislocation density [21,22]. The dislocation density decreases with increase of film thickness. The increase in peak intensity and decrease of FWHM is due to the improvement in the crystallinity and a reduction in the microstrain [21]. It is observed that the grain size increases continuously with increased film thickness and reached a maximum value of 44.6 nm for a thickness of 320 nm. Similar thickness dependence of the microstructural parameters on the deposition of other materials has been reported [22,23].

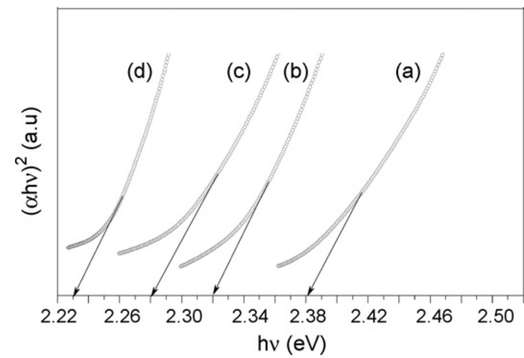

Fig. 2. $(\alpha h\nu)^2$ vs $h\nu$ plot of ZnTe films of different thickness (a) 110 nm (b) 180 nm (c) 230 nm (d) 320 nm.

The variation of % transmittance (T%) with wavelength was studied for the ZnTe films of different thicknesses and is shown in Fig. 2. Interference fringes are observed in these films which confirm the formation of smooth and uniform films. The onset of absorption is observed in the range 500–650 nm depending upon the thickness.

The transmittance spectra were used to calculate the absorption coefficient (α) at different wavelengths using the following relation:

$$T = \exp(-\alpha t)$$

where t is the film thickness and T is the transmittance of the film at a particular wavelength.

To determined the band gap E_g, we have used Tauc et al.'s plot [24] where the absorption coefficient α is a parabolic function of

Table 1
Lattice parameter, grain size, strain, stress and dislocation density of ZnTe films of different thicknesses deposited at 300 °C substrate temperatures.

Thickness (nm)	Lattice parameter "a" (Å)	Grain size (nm)	Stress (dyne cm^{-2}) ($\times 10^{10}$)	Strain ($\times 10^{-4}$)	Dislocation density ($\times 10^{16}$ cm^{-3})
110	6.084	12.1	2.15	9.4	0.247
180	6.089	24.2	−1.20	7.1	0.052
230	6.092	38.2	−0.90	4.2	0.041
320	6.098	44.6	−1.78	1.4	0.027

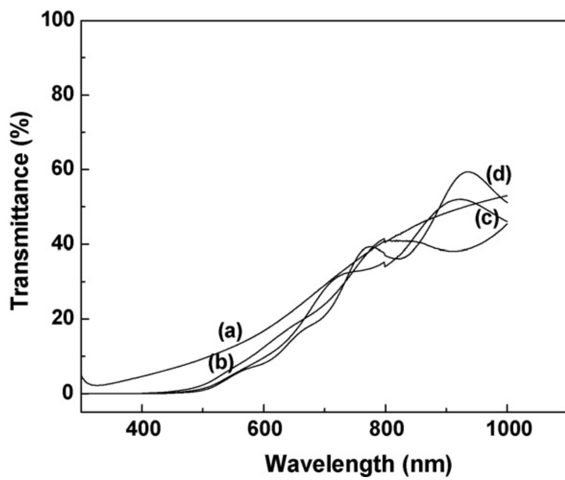

Fig. 3. Transmission spectra of ZnTe films of different thickness (a) 110 nm (b) 180 nm (c) 230 nm (d) 320 nm.

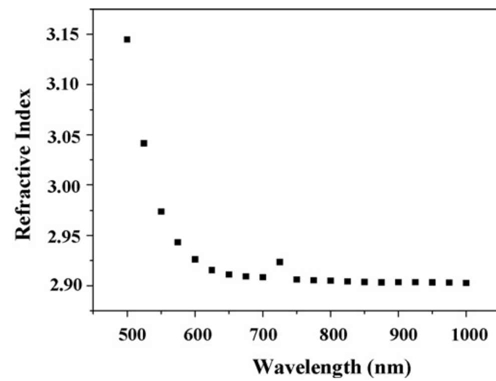

Fig. 4. Refractive index graph for the ZnTe films with thickness 320 nm.

the incident energy and optical band gap E_g is given by

$$\alpha = \frac{A(h\nu - E_g)^\gamma}{h\nu}$$

where A is the function of refractive index of the material, reduced mass and speed of light, ν is the transition frequency and the exponent γ characterizes the nature of band transition between the valence band and the conduction band. The band gap can be obtained from extrapolation of the straight-line potion of the $(\alpha h\nu)^\gamma$ vs $h\nu$ plot to $\alpha = 0$. A very high value of absorption co-efficient ($10^4\ \text{cm}^{-1}$) is observed for all the films. Plots of $(\alpha h\nu)^2$ vs $h\nu$ (Fig. 3) yielded band gap values in the range 2.38–2.23 eV as the thickness of the films increased from 110 to 320 nm. The lower value of the band gap at higher film thickness is due to the large grain size developed at higher thickness. Fig. 3 presents the optical transmittance spectra of the ZnTe films of different thickness. The refractive index was calculated using the interference maxima and minima observed at a wavelength from the transmission spectra by the envelope method [22,23] employing the following equations:

$$n = [N + (N^2 - n_s^2)]^2$$

$$N = \frac{n_s^2 + 1}{2} + \frac{2n_s(T_{max} - T_{min})}{T_{max}T_{min}}$$

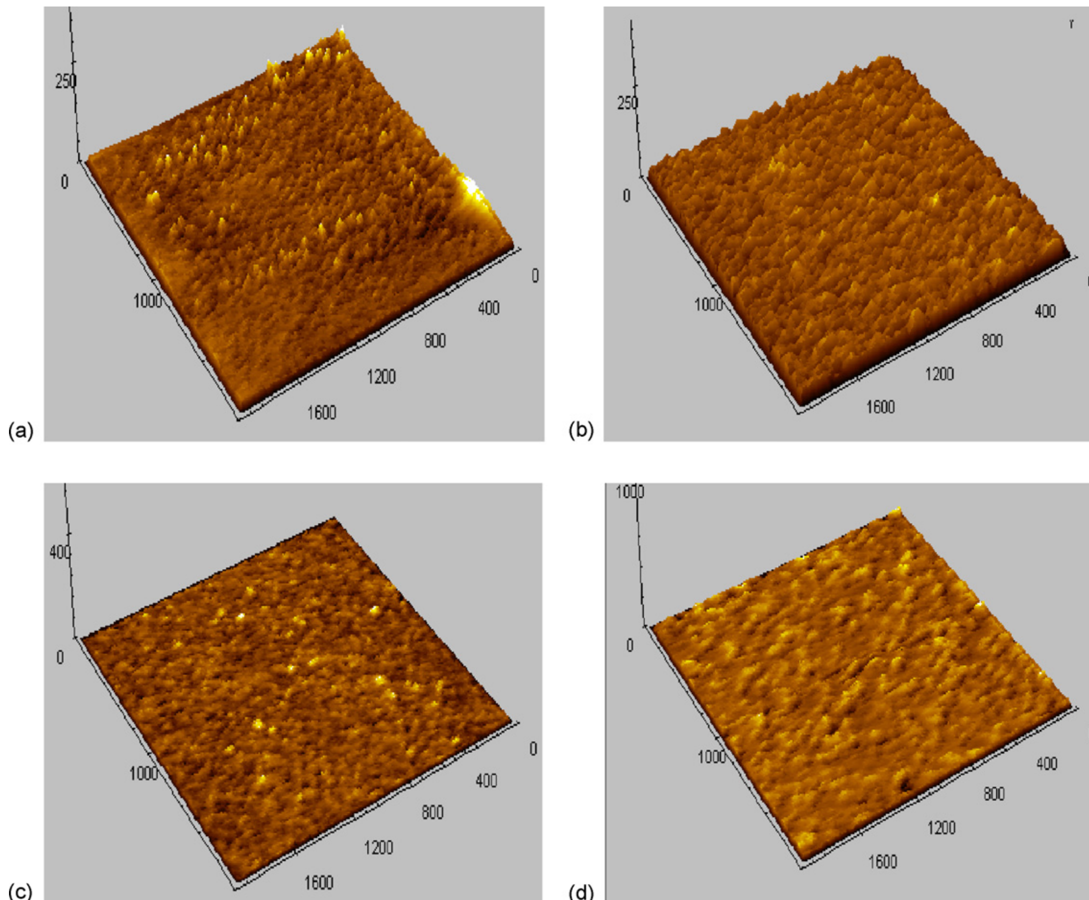

Fig. 5. Atomic force micrographic images of ZnTe films of different thickness (a) 110 nm (b) 180 nm (c) 230 nm (d) 320 nm.

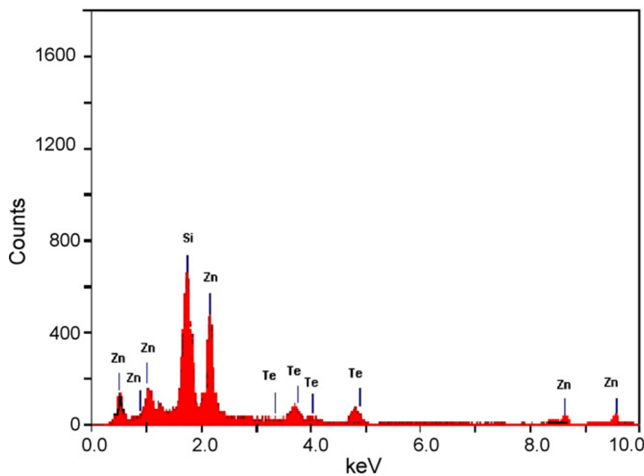

Fig. 6. EDAX spectra of 320 nm thick ZnTe films.

where n_s is the refractive index of the substrate, T_{max} and T_{min} are the maximum and minimum transmittances at the same wavelength in the fitted envelope curve on a transmittance spectrum.

The variation of refractive index with wavelength for the ZnTe film of thickness 230 nm is shown in Fig. 4. The refractive index decreases with increasing wavelength. The values of refractive index are constant in the near infrared region. The refractive index values calculated at a wavelength of 650 nm are 2.34, 2.72, 2.84 and 2.92 for the films of different thickness 110, 180, 230 and 320 nm, respectively. These values are comparable to earlier reports [25].

Surface morphology of the ZnTe films deposited with different thickness was studied by atomic force microscope (AFM) and the AFM micrographs are shown in Fig. 5. The presence of nanocrystallites is evident from the figures. The grain size values increased from about 70 to 150 nm and the root mean square (RMS) value of the roughness decreased 2.1–0.9 nm with increase of film thickness.

Composition of the films were estimated from energy dispersive analysis of X-rays (EDAX). The ratio of Zn:Te are about 48.3:51.7, 49.1:50.9, 49.0:51.0 and 49.5:50.5 for the films of different thickness 110, 180, 230 and 320 nm (Fig. 6).

Variation of resistivity with temperature was measured in the range between 27 and 150 °C (Fig. 7) for the ZnTe films with

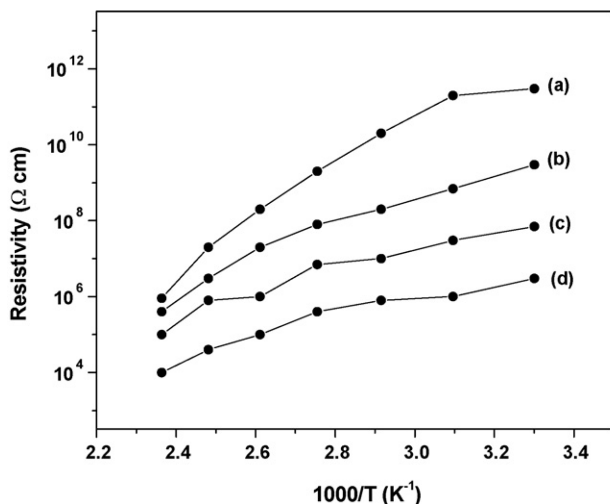

Fig. 7. Variation of resistivity with temperature for ZnTe film with different thickness (a) 110 nm (b) 180 nm (c) 230 nm and (d) 320 nm.

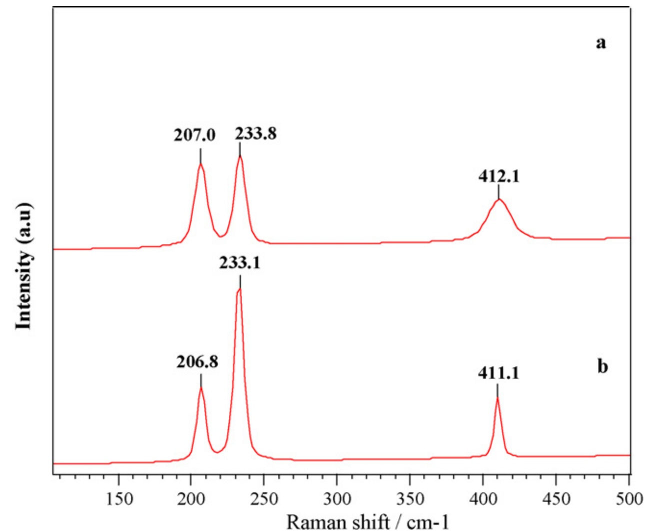

Fig. 8. Raman spectra for the ZnTe films deposited with different thicknesses (a) 110 nm (b) 320 nm.

different thickness. It is observed that the resistivity decreases continuously with increasing temperature. This corresponds to a thermally activated conduction mechanism in the ZnTe films. The resistivity can be represented by

$$\rho = \rho_0 \exp\left(\frac{-\Delta E_\sigma}{K_B T}\right)$$

where ΔE_σ is the activation energy, T is the tempertature, K is the Boltzmann constant. The plot exhibits two slopes, one between 27 and 60 °C and the other between 60 and 150 °C. The low activation energies are due to the high resistance of the samples with smaller film thickness. When the thickness increases, the activation energy also increases in the range 0.0057–0.0154 and 0.0158–0.0232 eV.

The room temperature Raman spectra of ZnTe films of thickness 110 and 320 nm deposited at a substrate temperature of 200 °C are shown in Fig. 8. The first order Raman scattering of a crystalline material with cubic structure usually shows two peaks corresponding to the transverse optic (TO) and longitudinal optic (LO) zone-centre phonon modes [26]. The observed peaks at about 206.8–207.0 and 411.1–412.1 cm^{-1} are assigned to the first order and second order ZnTe LO phonon scattering respectively. The peak at 233.7 eV could not be associated either with ZnTe or Te precipitates. Interestingly, the full width at half maximum (FWHM) of the LO peaks are decreasing with increasing thickness as observed from the broad and sharp peaks in Fig. 8a and b, respectively. This may be due to the increased grain size with thickness of the ZnTe films already demonstrated by the XRD and AFM results.

Photoluminescence study can provide information on the presence of native defects, impurities and structural defects [27]. PL spectra were recorded for the nanocrystalline ZnTe films with different thickness and Fig. 9 shows the PL emission spectra of ZnTe film with thickness 320 nm. The emission peaks in the spectra are separated in to three distinct regions. They are assigned to the radiative recombination of excitons bound to neutral acceptor (BE between 425 and 510 nm), free to a neutral acceptor (FA between 515 and 550 nm) and a donor–acceptor pair (DAP between 560 and 600 nm) [28]. The peak at 485.6 nm may be due to the recombination of excitons bound to neutral shallow acceptors. The peak position at 531.7 nm corresponds to a band gap value of 2.33 eV which is very close to the value of 2.33 eV for the nanocrystalline ZnTe film of thickness 320 nm. This emission peak is assigned to the radiative carrier recombination process of band-to-band transition [29]. The peaks observed between 562 and 592 nm are related to the

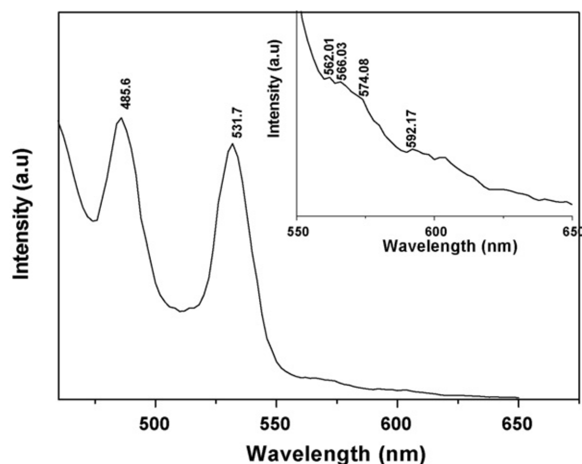

Fig. 9. PL emission spectra of 320 nm thick ZnTe film.

emission processes dominated by a 'DAP' band and located within the reported 2.10–2.27 eV energy interval, which may be ascribed to a recombination involving a shallow donor and an acceptor complex [30,31]. These PL observations confirm that ZnTe films with nano grains deposited here are of high purity and can be used for developing luminescence devices.

4. Conclusion

The ZnTe thin films with nano grains were deposited onto the glass substrates kept at 300 °C. The results of this study indicate that uniform and device quality ZnTe films with cubic structure can easily be deposited by the EB evaporation technique. Optical studies showed direct band gap value in the range of 2.23–2.38 eV which are found decreasing with the increase of film thickness. The grain size was in the range 70–150 nm as observed from AFM studies. Raman scattering and PL results confirmed the nano crystalline nature of the deposited ZnTe films.

References

[1] K. Sato, T. Asahi, M. Hanafusa, A. Noda, A. Arakawa, M. Uchida, O. Oda, Y. Yamada, T. Taguchi, Phys. Status Solidi A180 (2000) 267.
[2] D. Rioux, D.W. Niles, H. Hochst, J. Appl. Phys. 73 (1993) 8381.
[3] C.X. Shan, X.W. Fan, J.Y. Zhang, Z.Z. Zhang, X.H. Wang, J.G. Ma, J. Vac. Sci. Technol. 20 (2002) 1886.
[4] A. Ueta, D. Hommel, Phys. Status Solidi A192 (2002) 177.
[5] K. Yoshino, A. Memon, M. Yoneta, K. Ohmori, H. Sato, M. Ohishi, Phys. Status Solidi (B) 229 (2002) 977.
[6] J.H. Chang, T. Takai, K. Godo, J.S. Song, B.H. Koo, T. Hanada, Phys. Status Solidi (B) 229 (2002) 995.
[7] Q. Guo, Y. Kume, Y. Fukuhara, T. Tanaka, M. Nishio, H. Ogawa, Solid State Commun. 141 (2007) 188.
[8] B. Spath, J. Fritsche, F. Sauberlich, A. Klein, W. Jaegermann, Thin Solid Films 480 (2005) 204.
[9] T. Ishizaki, T. Ohtomo, A. Fuwa, J. Electrochem. Soc. 151 (2004) C161.
[10] T. Ishizaki, N. Saito, O. Takai, S. Asakura, K. Goto, A. Fuwa, Electrochim. Acta 50 (2005) 3509.
[11] K. Yoshino, A. Memon, M. Yoneta, K. Ohmori, H. Saito, M. Ohishi, Phys. Status Solidi (B) 229 (2002) 977.
[12] K. Sato, M. Hanafusa, A. Noda, A. Arakawa, M. Uchida, T. Asahi, O. Oda, J. Cryst. Growth 214/215 (2000) 1080.
[13] D. Rioux, D.W. Niles, H. Hochst, J. Appl. Phys. 73 (12) (1993) 8381.
[14] K. Liu, H. Kang, T. Kim, X.-C. Zhang, Appl. Phys. Lett. 81 (2002) 4115.
[15] A. Erlacher, B. Ullrich, Semicond. Sci. Technol. 19 (2004) L9.
[16] B. Ullrich, A. Erlacher, E.O. Danilov, Semicond. Sci. Technol. 19 (2004) L111.
[17] A. Erlacher, H. Miller, B. Ullrich, J. Appl. Phys. 95 (2004) 2927.
[18] A. Erlacher, B. Ullrich, R.J. Konopinski, H.J. Haugan, Proc. SPIE 5723 (2005) 179.
[19] A.M. Salem, T.M. Dahy, Y.A. El-Gendy, Physica B 403 (2008) 3027.
[20] C.X. Shan, X.W. Fan, J.Y. Zhang, et al., J. Vac. Sci. Technol. A—Vac. Surf. Films 20 (2002) 1886.
[21] N. El-Kadry, A. Aahour, S.A. Mohamoud, Thin Solid Films 269 (1995) 112.
[22] R. Swanepoel, J. Phys. E 16 (1983) 1214.
[23] J.E. Ramirez- Malo, E. Marquez, P. Villares, R. Jimenez-Garay, Mater. Lett. 17 (1997) 327.
[24] J. Tauc, R. Grigorvici, A. Vancu, Phys. Status Solidi 15 (1966) 627.
[25] A.E. Merad, M.B. Kanoun, G. Merad, J. Cilat, H. Aourag, Mater. Chem. Phys. 92 (2005) 333.
[26] E. Rudiger, J. Alvareg–Garcia, I. Luck, J. Klaer, R. Scheer, J. Phys. Chem. Solids 64 (2003) 1977.
[27] C. Morhain, E. Tournie, G. Neu, C. Ongaretto, J.P. Faurie, Phys. Rev. 54 (1996) 4714.
[28] K. Yoshino, M. Yoneta, T. Yabe, K. Ohmori, H. Saito, M. Ohisihi, Physica B 340–342 (2003) 254.
[29] A. Ebina, T. Takahashi, J. Cryst. Growth 59 (1982) 432.
[30] K. Wolf, A. Naumov, T. Reisinger, M. Kastner, H. Stanzl, W. Kuhn, K.W. Gebhardt, J. Cryst. Growth 135 (1994) 113.
[31] P. Paiano, P. Prete, N. Lovergine, A.M. Manicini, Cryst. Res. Technol. 40 (2005) 1011.